X-ray emission spectroscopy to study ligand valence orbitals in Mn coordination complexes

Grigory Smolentsev[†,*], **Alexander V Soldatov**[†], **Johannes Messinger**[‡,1], **Kathrin Merz**[‡], **Thomas Weyhermüller**[‡], **Uwe Bergmann**[@], **Yulia Pushkar**[∀], **Junko Yano**[#], **Vittal K. Yachandra**[#], and **Pieter Glatzel**[§,*]

[†]Faculty of Physics and Research center for Nanoscale Structure of Matter, Southern Federal University, 344090 Rostov-on-Don, Russia

[‡]Max-Planck Institute for Bioinorganic Chemistry, Stiftstr. 34-36, 45470 Mülheim, Germany

[@]Stanford Synchrotron Radiation Laboratory, P.O. Box 20450 Stanford, 94309 CA, USA

[∀]Department of Physics, Purdue University, West Lafayette, IN, USA

[#]Physical Biosciences Division, Lawrence Berkeley National Laboratory, Berkeley, CA, USA

[§]European Synchrotron Radiation Facility, 6, rue Jules Horowitz, 38043 Grenoble, France

Abstract

We discuss a spectroscopic method to determine the character of chemical bonding and for the identification of metal ligands in coordination and bioinorganic chemistry. It is based on the analysis of satellite lines in x-ray emission spectra that arise from transitions between valence orbitals and the metal ion 1s level (valence-to-core XES). The spectra, in connection with calculations based on density functional theory (DFT), provide information that is complementary to other spectroscopic techniques, in particular x-ray absorption (XANES and EXAFS). The spectral shape is sensitive to protonation of ligands and allows ligands, which differ only slightly in atomic number (e.g. C, N, O...), to be distinguished . A theoretical discussion of the main spectral features is presented in terms of molecular orbitals for a series of Mn model systems: $[Mn(H_2O)_6]^{2+}$, $[Mn(H_2O)_5OH]^+$, $[Mn(H_2O)_5NH_2]^+$ and $[Mn(H_2O)_5NH_3]^{2+}$. An application of the method, with comparison between theory and experiment, is presented for solvated Mn^{2+} ion in water and three Mn coordination complexes, namely $[LMn(acac)N_3]BPh_4$, $[LMn(B_2O_3Ph_2)(ClO_4)]$ and $[LMn(acac)N]BPh_4$ where L represents 1,4,7-trimethyl-1,4,7-triazacyclononane, acac stands for the 2,4-pentanedionate anion and $B_2O_3Ph_2$ represents the 1,3-diphenyl-1,3-dibora-2-oxapropane-1,3-diolato dianion.

1. Introduction

Identification of ligands coordinating metal ions and understanding their electronic structure is a fundamental problem in transition metal and bioinorganic chemistry. The degree of protonation of the ligand is important for hydrolysis reactions and mechanisms of hydrolytic

smolentsev@yandex.ru, glatzel@esrf.fr.
[1]Present address: Department of Chemistry, Umeå University, S-90187 Umeå, Sweden

enzymes actions such as carbonic anhydrase[2], dimethylargininase[3], metallo-β-lactamases[4], haloperoxidases[5] and many others. In oxidative reactions, for example in CytP450 chemistry or the oxygen-evolving Mn_4Ca complex in Photosystem II, the question arises whether reactive oxo-species (metal=O) exist or whether there is an oxo radical or water or a hydroxo group[6]. Furthermore, the structure at the active site of metalloproteins often remains elusive despite the existence of published crystal structures since possible uncertainties of atomic positions from protein crystallography can be in the range 0.1-0.3 Å[7,8] up to 0.5 Å[9]. The extended x-ray absorption fine structure (EXAFS) can provide valuable information but is limited when distinguishing between ligands with similar atomic numbers[10].

There are many traditional methods to experimentally investigate metal ligands. Nuclear magnetic resonance (NMR), electron nuclear double resonance (ENDOR), infra-red (IR), ultra-violet and visible (UV-Vis) spectra give characteristic signatures that allow the ligands to be identified. However, application of these methods is limited in some cases. X-ray absorption spectroscopy - especially analysis of the fine structure in the extended part (EXAFS) - is a well-known technique for probing the local atomic structure around a specific atom in condensed systems (e.g. for reviews see refs[11,12]) . The technique enables the measurement of bond lengths with an accuracy of ~0.02 Å in systems without long-range order. Recent developments in effective computational algorithms used for fitting the near-edge part of absorption spectra (XANES)[13,14] will probably allow one of the important limitations of EXAFS to be overcome, namely low sensitivity to bond angles. Nevertheless, x-ray absorption techniques have clear limitations. For one, it is practically impossible to distinguish neighbouring atoms with slightly different atomic number (for example C, O, N). Also, H atoms are in most cases invisible in EXAFS and can be identified in XANES only in very particular cases[15,16]. Therefore information about ligand protonation can be extracted only indirectly on the basis of correlations between bond lengths and ligand type[17].

X-ray emission spectroscopy (XES) (for review see e.g. ref[18,19]) offers a variety of techniques directly addressing problems concerning the electronic structure. For example, electron transitions between the metal atom 3p and 1s orbitals (Kβ lines) in 3d transition metal complexes allow the local atomic spin state to be determined[20-22]. The spin-sensitivity arises in this case from an intra-atomic interaction between the 3p and 3d shells. The 3d orbital configuration can be studied directly by observing L absorption edges and emission lines[19]. However, such experiments in the soft x-ray region (hν < 1000 eV) require high vacuum conditions and thus pose limitations with respect to sample environment. X-ray induced radiation damage to biological samples, in particular to metal centers and metal clusters increases dramatically at soft x-ray energies, limiting the application of technique for such samples[23]. In contrast, XES measurements performed at higher energies are very promising for metalloproteins[24]. Interpretation of these spectra is usually based on multiplet theory[25] due to the localized character of the orbitals that are involved in the transitions.[26,27]

Here we present an analysis of the x-ray emission lines just below the Fermi level after creation of a 1s core hole (valence-to-core XES) in Mn complexes. These weak features in the high energy part of XES have been known for many years[28] and have been denoted Kβ" and K$\beta_{2,5}$. The interest in them has increased due to the development of high-resolution spectrometers in the hard x-ray range at synchrotron radiation sources. The hard x-ray probe (hν > 5 keV) has the advantage of very few restrictions with respect to the sample environment. A number of previous studies exist[29-35], most notably perhaps the study of a series of Mn model systems with different ligands[36, 37]. A quantitative interpretation of the Kβ satellites using density functional theory (DFT) proved the feasibility and potential of this approach[38].

The formal electronic configuration in the final state of the x-ray emitting transition is identical to valence electron photoemission: X-ray photoemission spectroscopy (XPS) and Ultraviolet

photoemission spectroscopy (UPS) also known as electron spectroscopy for chemical analysis (ESCA). XES and XPS both test the occupied electron orbitals (in contrast to XAS) and thus provide similar information with the latter being a standard tool for chemical characterization. However, there are some important differences between the two techniques. XES is a strictly element specific probe, i.e. only electron density at the metal site (including the ligands) is probed with a considerably simpler analysis than resonant XPS experiments. The selection rules for electron transitions in K-XES only allow for orbitals to be detected that have *p*-contribution with respect to the metal atom. Also ultra high vacuum conditions are not required for XES, unlike for standard XPS experiments.

In the present paper we discuss in detail the information about the local chemical arrangement in 3d transition metal systems that can be gained using valence-to-core XES. The applicability and thus importance of this approach is due to the fact that the spectra can be successfully modeled by means of ground state DFT calculations. With a growing number of experimental stations at synchrotron radiation sources worldwide the technique becomes readily accessible, with considerable potential for the characterization of the electronic structure in metal complexes.

2. Theoretical Modeling

Valence-to-core XES were calculated numerically by integrating matrix elements between core-level and valence band molecular orbitals:
$$I(E_i) \sim \sum_{j=1}^{3} \left| \langle \Psi_{1s} | \vec{e}_j \vec{r} | \Psi_i \rangle \right|^2$$
where Ψ_{1s} and Ψ_i are wave functions corresponding to the core 1s state and valence state i with energy E_i and $\vec{e}_j$ is a set of three orthogonal unit vectors. The spectra corresponding to the unit vectors may not be identical depending on the local symmetry. This can give rise to a linear dichroism in single crystal samples as demonstrated by Dräger et al[37] and Bergmann et al.[38] All spectra shown here were obtained by summing over all unit vectors since the measurements were performed on polycrystalline samples. Isosurface plots are shown to illustrate the molecular orbitals. They correspond to the same value of the wave function ±0.03 and colored according to their sign.

Subsequent Lorentzian broadening of the spectrum (2 eV) was performed whilst accounting for the core level width and experimental resolution. Wavefunctions and orbital energies were calculated using the Amsterdam Density Function program suite (ADF2006.01)[39,40] within DFT. The electronic configuration of the molecule was described by an uncontracted double-ξ basis set of Slater-type orbitals. Energies were calculated using Perdew-Wang exchange correlation potential[41,42] within the generalized gradient approximation. A fundamental problem in inner-shell spectroscopy is to correctly account for the influence of the hole in a core electron level on the valence orbitals. The effect of the core-hole was considered within a simple Z+1 approximation and a relative energy scale was used in all calculations, i.e. the calculated energy scale was shifted by 6548 eV to correspond to the experiment. We found little influence of the core hole on the spectral shape. This observation will be addressed in the discussion section (*vide infra*).

XANES spectra were simulated using the self-consistent full multiple scattering FEFF8.2 code[43]. The Hedin-Lunqvist potential was employed to calculate the exchange part. Both multiple scattering and self-consistency of the potential were performed for all atoms of the molecules. Default values were used for all other parameters.

3. Experimental

The measurements were performed at beamline ID26 of the European Synchrotron Radiation Facility (ESRF). The incident energy was selected by means of a cryogenically cooled pair of Si crystals with a (111) orientation. The energy was tuned to 6.6 keV which is above the Mn K-edge but below the KL threshold for 1s2p double electron excitations that considerably affect the Kβ satellite line shape.[44] Higher harmonics were rejected by two Si mirrors operating in total reflection. Using the fundamental undulator peak, the maximum incident flux was 10^{13} photons/sec. The sample was oriented at 45 degrees with respect to the incident beam and the beam size on the sample was 0.5 mm horizontal and 1 mm vertical.

The x-ray emission was measured by means of a spherically bent (R=1000 mm) Si wafer with (4,4,0) orientation arranged in a Rowland geometry with an avalanche photodiode (APD) as the x-ray photon detector. The energy bandwidth of the emission spectrometer is 0.8 eV at 6.52 keV. The scattering plane is horizontal with the analyzer crystal positioned at 90 degrees scattering angle, i.e. along the polarization vector of the linear polarized incident x-ray beam.

Careful radiation damage studies were performed. Under the conditions of the experiment, damage was observed starting from 10 seconds of illumination. The evolution of the damage with time showed little dependence on the temperature and the measurements were thus performed in ambient conditions. The x-ray illumination time per beam spot on the sample was kept below the time limit where damage was observed.

The valence-to-core transitions are superimposed on a background that is due to the strong K$\beta_{1,3}$ line at lower emission energies. This background was subtracted by fitting Voigt line profiles to the K$\beta_{1,3}$ line. A small error due to the background subtraction may occur in the Kβ" region because the valence-to-core XES signal is weaker by a factor 2-3 compared to the background.

Polycrystalline samples of [LMn(acac)(N$_3$)]BPh$_4$, [LMn(B$_2$O$_3$Ph$_2$)(ClO$_4$)] and [LMn(acac) N]BPh$_4$ were prepared according to published procedures.[45,46] A solution of MnCl$_2$ in water (0.4 M) was measured in a jet stream.

4. Results and discussion

We discuss in section 4.1. the sensitivity of valence-to-core XES to substitution of the metal ligand on the basis of DFT calculations for 6-coordinated Mn complexes. This is compared to the sensitivity of XANES spectra. In section 4.2 an interpretation of the spectral features for these model molecules is given in terms of molecular orbitals. An application to real systems is presented in section 4.3. The experimentally observed trends in the spectra are interpreted using DFT.

4.1 Chemical sensitivity of the valence-to-core XES

Two critical limitations of x-ray absorption spectroscopy (XAS) are the low sensitivity to H atoms and the inability to distinguish between ligands with similar atomic numbers. We have performed calculations for a series of 6-coordinated model complexes of Mn: [Mn(H$_2$O)$_6$]$^{2+}$, [Mn(H$_2$O)$_5$OH]$^+$ and [Mn(H$_2$O)$_5$NH$_3$]$^{2+}$ in order to test the sensitivity of the valence-to-core XES method. The spectral shapes of XANES and XES are expected to be sensitive to two main effects: substitution of the ligand and rearrangement of the local structure. In order to separate the effect these factors have on the XES spectra, we considered two variations in molecule geometry. Firstly the inter-atomic distances were optimized using DFT, and secondly the Mn-ligand distances were kept fixed for all systems (five equal Mn-OH$_2$ distances of 2.17 Å, and

one short Mn-OH/OH$_2$ or Mn-NH$_3$ distance of 2.00 Å). Optimization of the local structure was performed without symmetry constrains.

Figure 1 shows a comparison between XES and XANES in [Mn(H$_2$O)$_6$]$^{2+}$, [Mn(H$_2$O)$_5$OH]$^+$ and [Mn(H$_2$O)$_5$NH$_3$]$^{2+}$ for two variations of the molecule geometry. We first discuss the spectra for the complexes with optimized geometries. Three peaks S1, P1 and P2 are observed in the XES of [Mn(H$_2$O)$_6$]$^{2+}$ (top-left of Fig. 1). A splitting occurs in the low-energy part (S1 and S2) for the [Mn(H$_2$O)$_5$OH]$^+$ complex, i.e. when a H$_2$O ligand is replaced by OH$^-$. The spectrum of [Mn(H$_2$O)$_5$NH$_3$]$^{2+}$ shows a weaker feature S2 In both complexes [Mn(H$_2$O)$_5$OH]$^+$ and [Mn(H$_2$O)$_5$NH$_3$]$^{2+}$ there are a few features marked as P3 at the high energy side. The corresponding XANES spectra (top-right of Fig. 1) show a clear difference between [Mn(H$_2$O)$_5$OH]$^+$ and the other two model compounds.

All XANES spectra with fixed Mn-ligand distances (bottom-right of Fig. 1) remain essentially identical when one of the six ligands is changed, while the XES spectra show clear features depending on the ligand type (Fig. 1 bottom-left). The XES peak positions are largely independent of the inter-atomic distances, changed within 0.2 Å limit and only the peak intensities are affected. This demonstrates a fundamental difference between XAS and XES. Inter-atomic distances influence the XAS K-edge shape, while the XES peak positions reflect the ligand type and the local symmetry. Valence-to-core XES can thus be used to determine the chemical nature of the different ligands even if they are spatially at the same positions. The model systems show that XES detects N/O substitution and the protonation state of the ligands.

Comparison of the XES spectra of the same molecules with different local geometries (spectra not shown) demonstrates that there is some sensitivity in the XES to the structural parameters. In particular the shape of the P3 peak significantly depends on the interatomic distance between Mn and N in the case of [Mn(H$_2$O)$_5$NH$_3$]$^{2+}$. Nevertheless, at the current level of interpretation of XES data, XANES and EXAFS provide a more robust way to investigate and determine bond lengths; therefore, this result highlights the complementary nature of the valence-to-core XES and XAS techniques.

4.2 Molecular orbital interpretation of spectral features

The results obtained from spectroscopic studies reflect the energy levels of the system, and it is often a challenge to arrive at conclusions with respect to the electronic structure and the chemical behavior based on the knowledge of energy levels alone. Successful theoretical modeling of the spectra paves the way for a more detailed interpretation of the experimental results and DFT is one such method. DFT allows us to understand the electron density in terms of molecular orbitals, thus providing a powerful tool for understanding the character of chemical bonds and the influence of ligands on the electronic structure of the central metal atom.

The results from the DFT calculations in Figure 2 (top) shows isosurfaces for the molecular orbitals (MO) contributing significantly to the XES spectrum of [Mn(H$_2$O)$_6$]$^{2+}$. There are a few analogous orbitals, that contribute to the same spectral features. The S1 peak results from transitions from a MO with *s*-character around the oxygen atoms. This feature is usually described as the Kβ" or "cross-over" peak[36]. The main contribution to this σ-bonding MO arises from O atomic orbitals (AO). The MO spreads over the entire H$_2$O ligand and thus some contribution also arises from H atoms. Different signs of the O wave functions lead to antisymmetric character of the MO around Mn. The weak shoulder labeled P1 arises from π-bonding between *p*-orbitals from O and Mn. The most intense peak P2 is assigned to σ-bonding between Mn and O *p*-orbitals. We note, that the assignment of the XES spectral features to ligand s and p orbitals is consistent with earlier studies[28, 37] and the DFT calculations are in nice agreement with experimental results on Mn oxides[36].

The XES spectra for the complex with an axial H_2O ligand substituted by OH^- contains contributions from the orbitals analogous to those shown for $[Mn(H_2O)_6]^{2+}$, but additionally there is feature from the oxygen *s*-like orbital of OH^- that forms peak S2 (Fig. 2, middle). The energy splitting between the orbitals forming S1 and S2 can be interpreted as a change in O *2s* binding energy as a proton has been removed from a H_2O ligand. This is consistent with the interpretation by Urch[47] and, consequently, XES has been proposed by Penner-Hahn and Bergmann as a tool to determine the degree of ligand protonation. We note that this energy splitting may be less pronounced if a larger molecule is considered, where charge can be screened by electron density on neighboring molecules. Two small peaks marked as P3 arise from p-orbitals of oxygen from the OH^- ligand. They are shifted to higher energies with respect to analogous orbitals of OH_2. There is also mixing of Mn d-states with O p-states for $[Mn(H_2O)_5OH]^+$ which is absent for $[Mn(H_2O)_6]^{2+}$. The mixing becomes possible due to the lowering of the symmetry around Mn upon substitution of H_2O by OH^-. It leads to the appearance of the peak at the highest energies. A similar mechanism occurs in $[Mn(H_2O)_5NH_3]^{2+}$ where the MO consisting of mainly N *s*-states from the NH_3 axial ligand gives rise to a S2 peak (Fig. 2 bottom). A feature, P3, corresponds to the transitions from a MO that contains contribution from *p*-like orbitals on three ligand molecules with the strongest contribution from the NH_3 ligand.

The MOs that significantly contribute to the valence-to-core XES spectral intensity are mainly localized on the ligands. This holds even for molecules without inversion symmetry and thus with mixing of *p*- and *d*-like orbitals with respect to the Mn atom. In other words, we do not observe strong contributions from Mn 3*d* orbitals and valence-to-core XES corresponds to the *p*-projected density of electronic states. This theoretical finding is at first surprising, but is confirmed in experiments (*vide infra* and ref [38]). The reason is that quadrupole, i.e. metal *3d* to *1s*, transitions are considerably weaker than dipole transitions. MOs that are localized mainly on the metal and therefore are expected to strongly contribute to the valence-to-core spectra, will in fact only be weakly visible because they are mostly formed by metal *3d* (*gerade*) orbitals. Valence-to-core XES thus arises from delocalized MOs with *p* (*ungerade*) symmetry with respect to the metal center.

A consequence of this delocalization of MOs that contribute to spectral intensity is that the spectra are only weakly sensitive to the effect of the core-hole. The core-hole is screened by the Mn valence electrons in the 3*d* shell (that we do not observe) and the ligand orbitals are not significantly affected by the change in effective nuclear charge on the Mn atom. Thus, ground state DFT calculations are expected to accurately model the valence-to-core XES spectra. This is demonstrated in the comparison between theory and experiment as described below. Another consequence of the low contribution of metal d-orbitals to the valence-to-core XES of coordination complexes is indirect sensitivity to the oxidation state. In the hypothetical case of oxidation state change without local structure modification the spectra will remain practically identical. Only the reconstruction of local geometry with subsequent formation of new molecular orbitals will lead to significant changes of the spectrum.

4.3 Comparison with experiment

Simulations of experimental valence-to-core XES spectra on simple 3d transition metal systems have been performed by various authors.[37,38] These studies form the basis of our detailed theoretical analysis above. In order to verify the approach we have measured the spectrum of a Mn^{2+} ion in water. Figure 3 shows a comparison with the theoretical data for $[Mn(H_2O)_6]^{2+}$. The main features that are observed experimentally are well reproduced in the theory. A slightly higher intensity of peak P1 and shoulder P3 in the experiment may be explained by dynamical disorder in the first coordination shell as well as the influence of more distant water molecules. In order to fully reproduce the experiment in the calculation it is

necessary to average a large number of spectra corresponding to the different snapshots of the solvent dynamic. Such calculations are beyond the scope of this work.

We furthermore measured and calculated the spectra for three complex coordination compounds: $[LMn(acac)N_3]BPh_4$, $[LMn(B_2O_3Ph_2)(ClO_4)]$ and $[LMn(acac)N]BPh_4$. Their structures have been determined by x-ray diffraction[45,46] (Fig. 4) and the formal oxidation state of the central manganese ion is known to be Mn(III) for $[LMn(acac)N_3]BPh_4$ (top) and $[LMn(B_2O_3Ph_2)(ClO_4)]$ and Mn(V) for $[LMn(acac)N_3]BPh_4$. They were chosen because of their structural similarities. The first two complexes have different numbers of O and N atoms near the metal ion. The systems are also suitable to study the influence of high coordination shells on the XES. No point group symmetry is present and strong orbital hybridization is thus expected.

The theoretical XES spectra are compared to experiment in Fig. 5. The overall shape of the experimental XES spectra is well reproduced in the calculations, corroborating the validity of our computational approach. A small discrepancy is observed in the low energy part of the S1 and P1 features. We ascribe this tentatively to multi-electron effects, which are not considered in our calculations. The influence of shake-off effects on valence-to-core XES was discussed previously[44]. A full treatment of multi-electron effects is computationally very demanding and currently not possible for molecular orbitals. Also, subtraction of the $K\beta_{1,3}$ background introduces some uncertainty in this spectral region.

The main differences between the spectra of the two Mn(III) systems are a sharpening and a shift towards higher energy of the S1 and P1 features. In order to clarify the origin of these effects we have analyzed the MOs that contribute to these features (Fig. 6). The split and rather broad S1 region in the spectrum of the $[LMn(acac)N_3]BPh_4$ system forms in a similar way as in $[Mn(H_2O)_5NH_3]^{2+}$ (Fig. 2, bottom). The MOs consist of mainly s-type AOs of the nearest O and N atoms. The orbitals that arise from oxygen contributions are between 2-3 eV lower in energy than those that correspond to nitrogen AOs resulting in a splitting of the S1 peak. A similar s-type nitrogen AO contributes to the S1 feature of the $[LMn(B_2O_3Ph_2)(ClO_4)]$ spectrum. However, substitution of the acac ligand by $B_2O_3Ph_2$ leads to a reconstruction of the atomic MOs with significant s-type oxygen character that is accompanied by a shift to higher energies. As a result, s-type oxygen and s-type nitrogen now have similar energies and the sharp S1 features are composed of a superposition of all nearest neighbor s-type orbitals. The substitution of the azide ligand with a perchlorate group is less important in the current case because the Mn-O distance relating to the perchlorate ligand is much longer (2.35 Å) compared with that for the $B_2O_3Ph_2$ (1.84 Å). The molecular orbital plots show clearly how the s orbitals of all three oxygen atoms hybridize via interactions with boron atoms. This effect occurs beyond the first coordination shell but nevertheless manifests itself in valence-to-core XES.

MOs contributing to the P1 region of the spectra are more complex (Fig. 6). For clarity, we show those parts of the MOs, which are far from the Mn atoms as a mesh. These parts of the MOs provide only a weak contribution to the valence-to-core XES spectral intensity and will not, therefore, be considered in detail in the following discussion. It is predominantly p-type orbitals from acac oxygens and from nitrogens in the axial azido group which contribute to the P1 peak for $[LMn(acac)N_3]BPh_4$.

The perchlorate group does not contribute to the spectral intensity of P1 in the case of $[LMn(B_2O_3Ph_2)(ClO_4)]$ as discussed above and the P1 peak is mainly formed by the $B_2O_3Ph_2$ group. MOs mainly consisting of O p-orbitals are higher in energy for the $B_2O_3Ph_2$ group of $[LMn(B_2O_3Ph_2)(ClO_4)]$ than for $[LMn(acac)N_3]BPh_4$. This explains the energy shift of the P1 feature between the spectra. A further analysis shows that the perchlorate group does give rise

to spectral intensity near the maximum of P2. Also, *sp*-hybridized orbitals of ClO_4 oxygen add intensity in the region around -17eV.

A rather weak effect upon substitution of the axial ligand is observed when comparing spectra of $[LMn(acac)N_3]BPh_4$ and $[LMn(B_2O_3Ph_2)(ClO_4)]$. The influence of the axial ligand becomes dominant when $[LMn(acac)N_3]BPh_4$ and $[LMn(acac)N]BPh_4$ are considered. A very strong peak S2 (see Fig 5) is observed in the case of $[LMn(acac)N]BPh_4$ that arises from the s-orbital of the axial nitrogen with a strong bond to Mn.

Qualitatively, valence-to-core XES spectra are sensitive to the chemical bonding character between the metal and nearest neighbor atoms and types of metal neighbors. The overall shape of the spectrum can be reproduced using a set of atomic coordinates that does not need to be determined with high precision. However, outer atoms, which influence the hybridization of ligand *p*-type states, can attract electronic density and thus modify the ligand electron configuration. Consequently, the entire coordination complex must be considered in a quantitative calculation of valence-to-core XES. The cluster size, i.e. the number of atoms required in XES calculations, is therefore similar to that typically used for XANES calculations (4.5-6 Å). In contrast to XANES simulations, we find that H atoms need to be included in calculations of valence-to-core XES spectra, because they participate in the overall character of the chemical bond. H atoms influence the spectral shape of XANES only weakly since the backscattering amplitude is low. This leads to the conclusion that H AOs contribute strongly to MOs that have energies in the region of valence-to-core XES spectra, but contribute only weakly to unoccupied orbitals in the XANES spectral region. Weak contribution from H atoms to XAS has previously been observed only in specific cases, for example at the O K-edge in water[48]. When analyzing the sensitivity of XES to the local geometry, we find only minor dependence on the bond angles. We do, however, observe an influence of the bond length on the intensity of the P1 and P2 peaks.

Conclusions

We have demonstrated the sensitivity of valence-to-core XES to the nature of the ligands present in *3d* transition metal systems. The technique can be used to identify both simple (such as water versus OH^-) and more complicated (acac versus $B_2O_3Ph_2$) ligands. The key advantage of this method as compared with x-ray absorption spectroscopy is the high sensitivity to the character of the chemical bonding. As a result, valence-to-core XES is able to detect the degree of ligand protonation as well as substitution of ligand atoms with others of similar atomic number (e.g., N for O).

We note that x-ray emission spectroscopy does not always require a synchrotron radiation source. Experiments using laboratory x-ray sources or even radioactive isotopes have been performed[18, 49-51]. Therefore the potential of this technique is high and of interest to many research groups.

Acknowledgments

References

[2]. Bergquist C, Fillebeen T, Morlok M, Parkin G. J. Am. Chem. Soc 2003;125:6189–6199. [PubMed: 12785851]

[3]. Stone EM, Costello AL, Tierney DL, Fasr W. Biochemistry 2006;45:5618–5630. [PubMed: 16634643]

[4]. Kaminskaia NV, Spingler B, Lippard SJ. J. Am.Chem. Soc 2000;122:6411–6422.

[5]. Zampella G, Fantucci P, Pecoraro VL, Geoia LD. J. Am. Chem. Soc 2005;127:953–960. [PubMed: 15656634]

[6](a). Green MT, Dawson JH, Gray HB. Science 2004;304:1653–1656. [PubMed: 15192224] (b) Su JH, Lubitz W, Messinger J. J. Am. Chem. Soc 2008;130:786–787. [PubMed: 18161970]

[7]. DePristo MA, de Bakker PLW, Blundell TL. Structure 2004;12:831–838. [PubMed: 15130475]

[8]. Tickle IJ, Laskowski RA, Moss DS. Acta Crystallogr., Sect. D: Biol. Crystallogr 1998;54:243–252. [PubMed: 9761889]

[9]. Kuriyan J, Karplus M, Petsko GA. Proteins: Struct., Funct., Genet 1987;2:1–12. [PubMed: 3447165]

[10]. Yano J, Kern J, Sauer K, Latimer MJ, Pushkar Y, Biesiadka J, Loll B, Saenger W, Messinger J, Zouni A, Yashandra V. Science 2006;314:821–825. [PubMed: 17082458]

[11]. Penner-Hahn JE. Coord. Chem. Rev 2005;249:161–177.

[12]. Strange RW, Ellis M, Hasnain SS. Coord. Chem. Rev 2005;249:197–208.

[13]. Smolentsev G, Soldatov A. J. Synchrotron Rad 2006;13:19–29.

[14]. Benfatto M, Longa S. Della. J. Synchrotron Rad 2001;8:1087–1094.

[15]. Soldatov AV, Della-Longa S, Bianconi A. Solid State Commun 1993;85:863–868.

[16]. Witjens LC, Bitter JH, van Dillen AJ, de Jong KP, de Groot FMF. Phys. Chem. Chem. Phys 2004;6:3903–3906.

[17]. Baldwin MJ, Stemmler TL, Riggs-Gelasco PJ, Kirk ML, Penner-Hahn JE, Pecoraro VL. J. Am. Chem. Soc 1994;116:11349–11356.

[18]. Glatzel P, Bergmann U. Coord. Chem. Rev 2005;249:65–95.

[19](a). de Groot FMF. Chem. Rev 2001;101:1779–1808. [PubMed: 11709999] (b) de Groot FMF. J. Electron Spectrosc. Relat. Phenom 1994;67:529–622.

[20]. Peng G, deGroot FMF, Haemaelaeinen K, Moore JA, Wang X, Grush MM, Hastings JB, Siddons DP, Armstrong WH, Mullins OC, Cramer SP. J. Am. Chem. Soc 1994;116:2914–2920.

[21]. Qian Q, Tyson TA, Kao CC, Croft M, Cheong SW, Greenblatt M. Phys. Rev. B 2000;62:13472–13481.

[22]. Rueff JP, Krisch M, Cai YQ, Kaprolat A, Hanfland M, Lorenzen M, Masciovecchio C, Verbeni R, Sette F. Phys. Rev. B 1999;60:14510–14512.

[23]. George SJ, Fu JX, Guo YS, Drury OB, Friedrich S, Rauchfuss T, Volkers PI, Peters JC, Scott V, Brown SD, Thomas CM, Cramer SP. Inorg. Chim. Acta 2008;361:1157–1165.

[24]. Messinger J, Robblee JH, Bergmann U, Fernandez C, Glatzel P, Visser H, Cinco RM, McFarlane KL, Bellacchio E, Pizarro SA, Cramer SP, Sauer K, Klein MP, Yachandra VK. J. Am. Chem. Soc 2001;123:7804–7820. [PubMed: 11493054]

[25]. de Groot F. Coord. Chem. Rev 2005;249:31–63.

[26]. Kotani A, Shin S. Rev. Mod. Phys 2001;73:203–246.

[27]. Demchenko DO, Liu AY, Kurmaev EZ, Finkelstein LD, Galakhov VR, Moewes A, Chiuzbăian SG, Neumann M, Kmety CR, Stevenson KL. Phys. Rev. B 2005;69:205105/1–205105/9.

[28]. Urch, DS. X-ray Emission Spectroscopy. In: Urch, DS., editor. Electron Spectroscopy, Theory, Techniques and Application. Vol. Vol. 3. Academic Press; New York: 1979. p. 1-39.

[29]. Ankudinov AL, Elam WT, Sieber JR, Rehr JJ. X-ray Spectrom 2006;35:312–318.

[30]. Uda E, Kawai J, Uda M. Nucl. Instrum. Methods Phys. Res., Sect. B 1993;75:24–27.

[31]. Uda M, Yamamoto T, Tatebayashi T. Nucl. Instrum. Methods Phys. Res., Sect. B 1999;150:55–59.

[32]. Nodwell E, Adamcyk M, Ballestad A, Tiedje T, Tixier S, Webster SE, Young EC, Moewes A, Kurmaev EZ, van Buuren T. Phys. Rev. B 2004;69:155210/1–155210/4.

[33]. Kurmaev EZ, Moewes A, Bureev OG, Nekrasov IA, Cherkashenko VM, Korotin MA, Ederer DL. J. Alloys Compd 2002;347:213–218.

[34]. Pandey RK, Mukamel S. J. Chem. Phys 2006;124:094106/1–094106/10.

[35]. Mukoyama T. Spectrochim. Acta, Part B 2004;59:1107–1115.

[36]. Bergmann U, Horne CR, Collins TJ, Workman JM, Cramer SP. Chem. Phys. Lett 1999;302:119–124.

[37]. Dräger, G.; Brümmer, O. Inner-Shell and X-Ray Physics of Atoms and Solids. Fabian, DJ.; Kleinpoppen, H.; Watson, LM., editors. Plenum Press; New York: 1980. p. 825-829.

[38](a). Bergmann U, Bendix J, Glatzel P, Gray HB, Cramer SP. J. Chem. Phys 2002;116:2011–2015. (b) Safonov VA, Vykhodtseva LN, Polukarov Yu. M. Safonova OV, Smolentsev G, Sikora M, Eeckhout SG, Glatzel P. J. Phys. Chem. B 2006;110:23192–23196. [PubMed: 17107164]

[39]. te Velde G, Bickelhaupt FM, van Gisbergen SJA, Guerra C. Fonseca, Baerends EJ, Snijders JG, Ziegler T. J. Comput. Chem 2001;22:931–967.

[40]. Guerra CF, Snijders JG, te Velde G, Baerends EJ. Theor. Chem. Acc 1998;99:391–403.

[41]. Perdew JP, Chevary JA, Vosko SH, Jackson KA, Pederson MR, Singh DJ, Fiolhais C. Phys. Rev. B 1992;46:6671–6687.

[42]. Perdew JP. Phys. Rev. B 1986;33:8822–8824.

[43]. Ankudinov AL, Ravel B, Rehr JJ, Conradson SD. Phys. Rev. B 1998;58:7565–7576.

[44]. Glatzel, P.; Bergmann, U.; de Groot, FMF.; Cramer, SP. X-Ray and Inner-Shell Processes. Bianconi, A.; Marcelli, A., editors. American Institute of Physics; Rome: 2002. p. 250-253.

[45]. Niemann A, Bossek U, Haselhorst G, Wieghardt K, Nuber B. Inorg. Chem 1996;35:906–915. [PubMed: 11666264]

[46]. Bossek U, Hummel H, Weyhermuller T, Wieghardt K, Russell S, van der Wolf L, Kolb U. Angew. Chem., Int. Ed. Engl 1996;35:1552–1554.

[47]. Urch DS. J. Phys. C 1970;3:1275–1291.

[48]. Bergmann U, Di Cicco A, Wernet P, Principi E, Glatzel P, Nilsson A. J. Chem. Phys 2007;127:174504/1–174504/5. [PubMed: 17994824]

[49]. Schnopper, HW.; Parratt, LG. Röntgenspektren und Chemische Bindung. Meisel, A., editor. Leipzig University Press; Leipzig: 1996. p. 314-324.

[50]. Meisel, A.; Leonhardt, G.; Szargan, R. X-Ray Spectra and Chemical Binding. Vol. Vol. 37. Springer-Verlag; New York: 1989. Springer Series in Chemical Physics

[51](a). Bergmann U, Glatzel P, de Groot FMF, Cramer SP. J. Am. Chem. Soc 1999;121:4926–4927. (b) Glatzel P, Bergmann U, de Groot FMF, Cramer SP. Phys. Rev. B 2001;64:045109/1–045109/10.

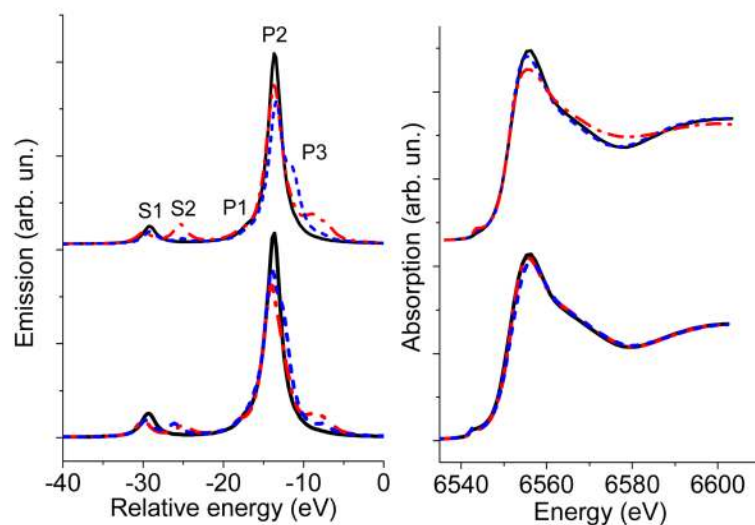**Figure 1.**
Theoretical valence-to-core XES (left panel) and Mn K-edge XANES (right panel) of [Mn (H$_2$O)$_6$]$^{2+}$ (black solid line), [Mn(H$_2$O)$_5$OH]$^+$ (red dash-dotted line) and [Mn(H$_2$O)$_5$NH$_3$]$^{2+}$ (blue dashed line). Spectra are shown with optimized local structures (top) and with fixed metal-ligand distances (bottom).
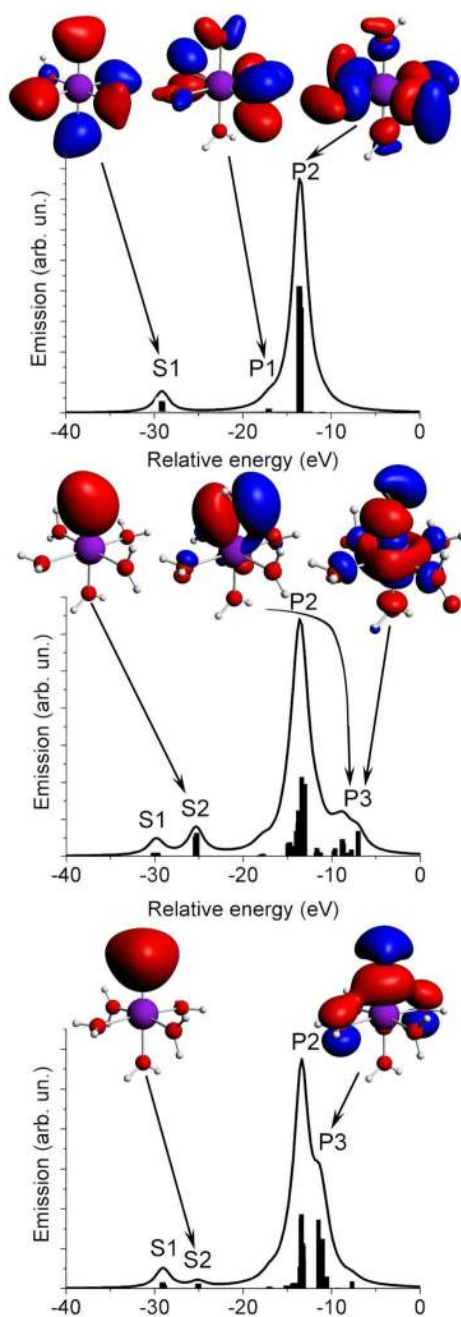
Figure 2.
Theoretical valence-to-core XES, with some important molecular orbitals contributing to the spectra of $[Mn(H_2O)_6]^{2+}$ (top), $[Mn(H_2O)_5OH]^+$ (middle) and $[Mn(H_2O)_5NH_3]^{2+}$ (bottom). Sticks show contributions of individual molecular orbitals. Isosurfaces are colored red (blue) for positive (negative) values of the wavefunction. The geometry of the molecule is shown with O (red), H (grey), N (blue) and Mn (magenta).
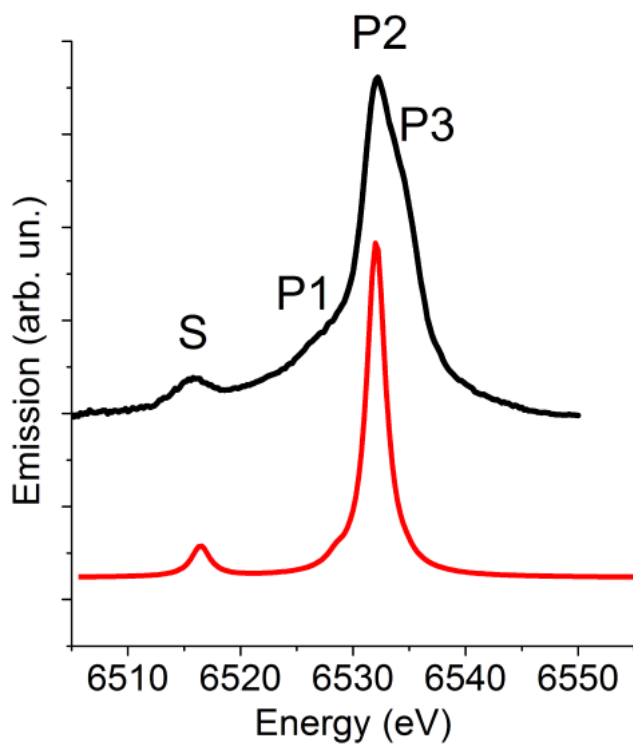
Fig. 3.
Experimental (top) valence-to-core XES of solvated Mn^{2+} ion in water and theoretical spectrum of $[Mn(H_2O)_6]^{2+}$ (bottom).
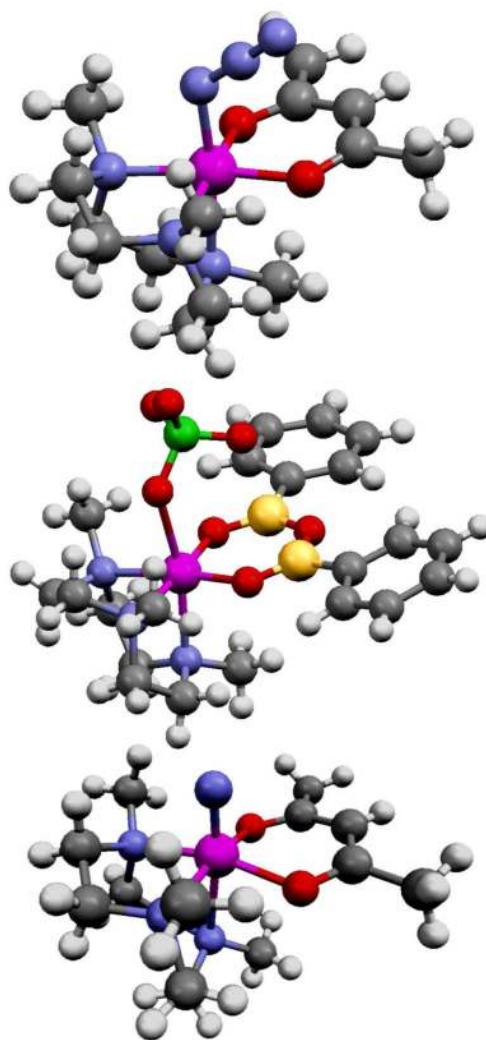
Figure 4.
Schematic representation of [LMn(acac)N$_3$]BPh$_4$ (top) and [LMn(B$_2$O$_3$Ph$_2$)(ClO$_4$)] (middle) and [LMn(acac)N] BPh$_4$ (bottom) with C (black), O (red), N (blue), B (yellow), Cl (green), H (grey) and Mn (magenta) atoms. Distant counter ion BPh$_4$ is not shown for the top and bottom structures.
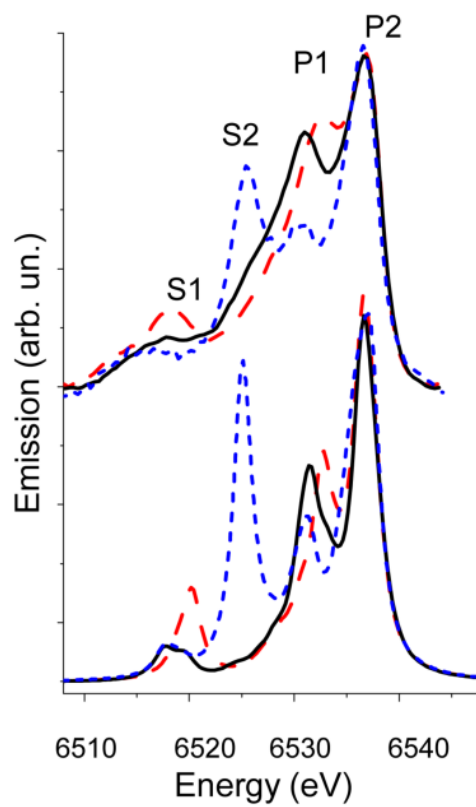
Figure 5.
Experimental (top) and theoretical (bottom) valence-to-core XES of [LMn(acac)N$_3$]BPh$_4$ (black solid lines), [LMn(B$_2$O$_3$Ph$_2$)(ClO$_4$)] (red dashed lines) and [LMn(acac)N]BPh$_4$ (blue short-dashed lines).

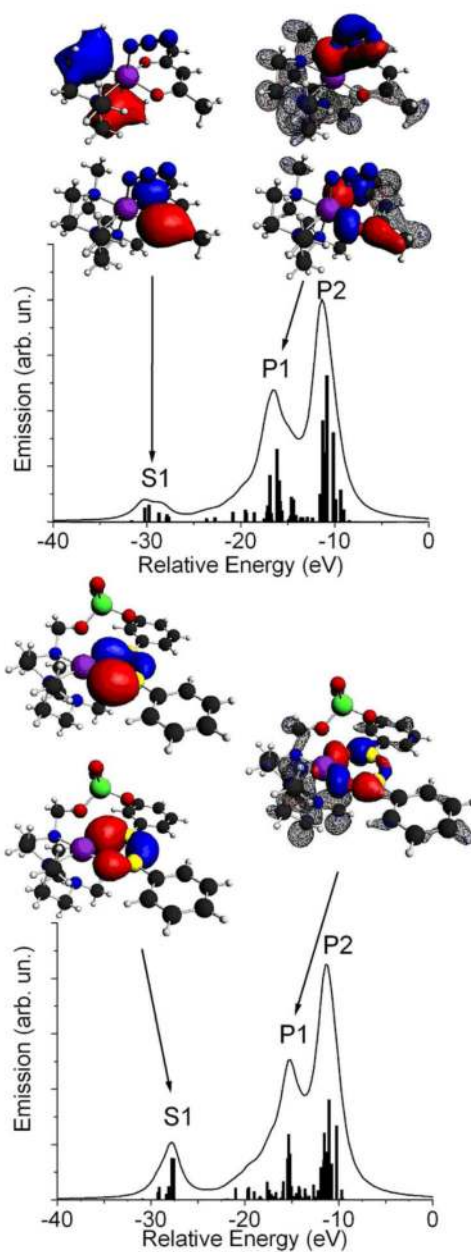**Figure 6.**
Theoretical valence-to-core XES and some important molecular orbitals contributing to the XES spectra of [LMn(acac)N$_3$]BPh$_4$ (top) and [LMn(B$_2$O$_3$Ph$_2$)(ClO$_4$)] (bottom). Sticks show contributions of individual molecular orbitals. Isosurfaces corresponding to the positive (red) and negative (blue) values of the wave function are plotted. Parts of the MOs are shown as a mesh for clarity. The geometry of the molecules is shown with O (red), N (blue), C (black), B (yellow), Cl (green), H (grey) and Mn (magenta) atoms.